562 J. Med. Chem. 2011, 54, 562–571
DOI: 10.1021/jm101004d

Journal of Medicinal Chemistry Article

# Inhibition of Lymphoid Tyrosine Phosphatase by Benzofuran Salicylic Acids

Torkel Vang,[†] Yuli Xie,[‡] Wallace H. Liu,[†] Dušica Vidović,[∥] Yidong Liu,[‡] Shuangding Wu,[†] Deborah H. Smith,[§] Alison Rinderspacher,[‡] Caty Chung,[∥] Gangli Gong,[‡] Tomas Mustelin,[†] Donald W. Landry,[‡] Robert C. Rickert,[†] Stephan C. Schürer,[∥,⊥] Shi-Xian Deng,[‡] and Lutz Tautz*,[†]

[†]*Infectious and Inflammatory Disease Center, Sanford-Burnham Medical Research Institute, 10901 North Torrey Pines Road, La Jolla, California 92037, United States,* [‡]*Department of Medicine, and* [§]*Department of Physiology and Cellular Biophysics, Columbia University, New York, New York 10032, United States,* [∥]*Center for Computational Science, University of Miami, Miami, Florida 33458, United States, and* [⊥]*Department of Pharmacology, Miller School of Medicine, University of Miami, Miami, Florida 33458, United States*

*Received August 4, 2010*

The lymphoid tyrosine phosphatase (Lyp, PTPN22) is a critical negative regulator of T cell antigen receptor (TCR) signaling. A single-nucleotide polymorphism (SNP) in the *ptpn22* gene correlates with the incidence of various autoimmune diseases, including type 1 diabetes, rheumatoid arthritis, and systemic lupus erythematosus. Since the disease-associated allele is a more potent inhibitor of TCR signaling, specific Lyp inhibitors may become valuable in treating autoimmunity. Using a structure-based approach, we synthesized a library of 34 compounds that inhibited Lyp with $IC_{50}$ values between 0.27 and 6.2 $\mu$M. A reporter assay was employed to screen for compounds that enhanced TCR signaling in cells, and several inhibitors displayed a dose-dependent, activating effect. Subsequent probing for Lyp's direct physiological targets by immunoblot analysis confirmed the ability of the compounds to inhibit Lyp in T cells. Selectivity profiling against closely related tyrosine phosphatases and in silico docking studies with the crystal structure of Lyp yielded valuable information for the design of Lyp-specific compounds.

## Introduction

Protein tyrosine phosphorylation is a key regulatory mechanism of signal transduction pathways and plays an extremely important role in many cellular processes that are characteristic of higher eukaryotes.[1,2] The spatially and temporally coordinated interplay of protein tyrosine kinases (PTKs[a]) and protein tyrosine phosphatases (PTPs) results in tyrosine phosphorylation and dephosphorylation of numerous cytosolic and transmembrane proteins. The importance of PTPs is highlighted by their implication in many human diseases, including cancer, cardiovascular, immunological, infectious, neurological, and metabolic diseases.[3−5]

The human lymphoid tyrosine phosphatase Lyp[6] is encoded by the *ptpn22* gene and is expressed exclusively by hematopoietic cells. The 105 kDa protein has an N-terminal catalytic domain that is highly similar to other tyrosine-specific classical nonreceptor-type PTPs. The central region, which is of unknown function, is followed by a C-terminal part that contains four proline-rich sequence motifs, termed P1−P4. Lyp has a critical negative regulatory role in T cell antigen receptor (TCR) signaling by acting immediately downstream of the TCR. Identified substrates of Lyp include the leukocyte-specific protein tyrosine kinase (Lck, Tyr-394), the immunoreceptor tyrosine-based activation motifs (ITAMs) of CD3/ζ-chains, the ζ-chain-associated protein kinase 70 (ZAP-70; Tyr-493), the guanine-nucleotide exchange factor Vav, and the valosine-containing protein (VCP).[7] Recently, a single-nucleotide polymorphism (SNP) in *ptpn22* was discovered to correlate with the incidence of type 1 diabetes[8] and was later confirmed and expanded to include rheumatoid arthritis, systemic lupus erythematosus, Graves disease, and other autoimmune diseases (reviewed in ref 5). The autoimmunity-predisposing allele of Lyp is a missense (C1858T) mutation, which changes amino acid residue 620 from arginine (Lyp*R620) to tryptophan (Lyp*W620). This change is significant because R620 is a critical residue in the P1 proline-rich motif that mediates binding to the Src homology 3 (SH3) domain of the PTK Csk.[8] Subsequent studies showed that the disease-predisposing Lyp*W620 is a gain-of-function mutant that suppresses TCR signaling much more effectively.[9] Thus, inhibition of Lyp may provide a new approach to treat autoimmunity.

Recently, a specific small-molecule inhibitor of Lyp I-C11[10] (**478**, Table 1) was reported, along with the cocrystal structure of the compound bound to Lyp's active site.[10] The X-ray coordinates clearly indicated a binding mode in which the inhibitor interacts with both the phosphate-binding pocket (catalytic pocket) and a nearby peripheral site. On the basis of the chemical structure of **478** and its interactions with Lyp, we report the design and evaluation of a library of 6-hydroxy-benzofuran-5-carboxylic acids (benzofuran salicylic acids),

*To whom correspondence should be addressed. Phone: (858) 646-3100, extension 3640. Fax: (858) 795-5412. E-mail: tautz@burnham.org.

[a] Abbreviations: Lyp, lymphoid tyrosine phosphatase; PTP, protein tyrosine phosphatase; PTK, protein tyrosine kinase; *p*Tyr, phosphotyrosine; TCR, T cell antigen receptor; ITAM, immunoreceptor tyrosine-based activation motif; IL-2, interleukin-2; NFAT, nuclear factor of activated T-cells; AP-1, activator protein 1; Lck, leukocyte-specific protein tyrosine kinase; ZAP-70, ζ-chain-associated protein kinase 70; SNP, single-nucleotide polymorphism; VCP, valosine-containing protein; SAR, structure−activity relationship; DiFMUP, 6,8-difluoro-4-methylumbelliferyl phosphate; DTT, dithiothreitol.

 Published on Web 12/29/2010 

**Table 1.** Synthesized Library of Benzofuran Salicylic Acids, Ordered by Their $IC_{50}$ Value for Lyp

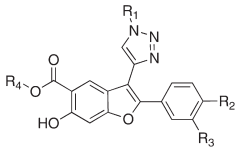

| # | R1 | R2 | R3 | R4 | IC50, μM | # | R1 | R2 | R3 | R4 | IC50, μM |
|---|---|---|---|---|---|---|---|---|---|---|---|
| **526** | 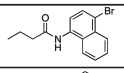 | Me | H | H | 0.27 | **523** | 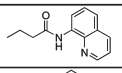 | Me | H | H | 1.11 |
| **584** | 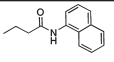 | MeO | H | H | 0.34 | **529** |  | Me | H | H | 1.18 |
| **586** | 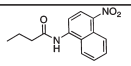 | MeO | H | H | 0.34 | **530** | 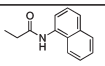 | Me | H | H | 1.35 |
| **525** | 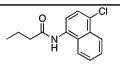 | Me | H | H | 0.38 | **480** | 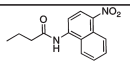 | H | H | H | 1.49 |
| **522** | 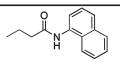 | Me | H | H | 0.41 | **532** | 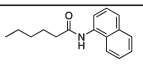 | Me | H | H | 1.80 |
| **619** | 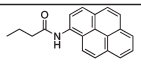 | Me | H | H | 0.48 | **531** | 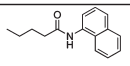 | Me | H | H | 2.01 |
| **630** | 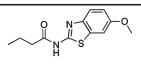 | H | Me | H | 0.52 | **496** | 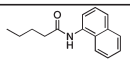 | H | H | H | 2.21 |
| **481** | 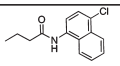 | H | H | H | 0.56 | **577** | 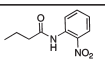 | H | Me | H | 2.35 |
| **636** | 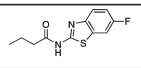 | H | Me | H | 0.61 | **499** | 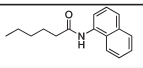 | H | H | H | 2.64 |
| **524** | 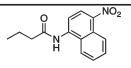 | Me | H | H | 0.64 | **491** | 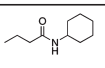 | H | H | H | 3.10 |
| **609** | 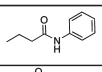 | H | Me | H | 0.65 | **479** | 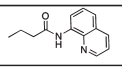 | H | H | H | 3.22 |
| **612** | 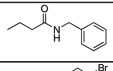 | H | Me | H | 0.65 | **527** | 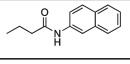 | Me | H | H | 3.44 |
| **482** | 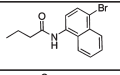 | H | H | H | 0.71 | **483** | 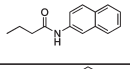 | H | H | H | 3.84 |
| **611** | 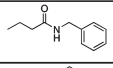 | H | H | H | 0.74 | **478** | 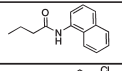 | H | H | H | 4.50 |
| **492** |  | H | H | H | 0.77 | **486** | 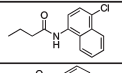 | H | H | Me | 4.86 |
| **528** | 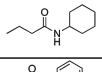 | Me | H | H | 0.90 | **604** | 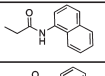 | H | Me | H | 5.02 |
| **495** | 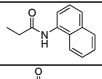 | H | H | H | 0.91 | **569** | 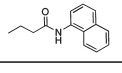 | H | Me | H | 6.20 |
| **610** | 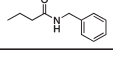 | Me | H | H | 0.97 | | | | | | |

which yielded compounds with substantially higher potency in inhibiting Lyp in vitro and in T cell-based assays.

## Results

**Structure-Based Design of a Library of Benzofuran Salicylic Acids.** On the basis of the structure of the published Lyp inhibitor **478**, we designed and synthesized a library of analogues with potentially higher inhibitory activity and selectivity for Lyp. According to the cocrystal structure of **478** and Lyp (Figure 1), the benzofuran salicylic acid moiety binds into the phosphate-binding pocket (catalytic pocket), whereas the distal naphthalene ring interacts with a nearby peripheral site, formed by Phe-28, Leu-29, Lys-32, and Arg-33. Interestingly, these residues are part of a second-site binding pocket in Lyp, corresponding to an equivalent phosphate-binding site previously identified in PTP1B.[11] In PTP1B this second site is important for substrate recognition[12] and has been targeted with small-molecule inhibitors.[13] We therefore chose a strategy in which we modified the naphthalene ring with various substituents or replaced it with different structural elements in order to generate compounds with enhanced binding affinity to this second site in Lyp. In addition, we introduced substituents at the phenyl ring that is attached to the benzofuran ring in the

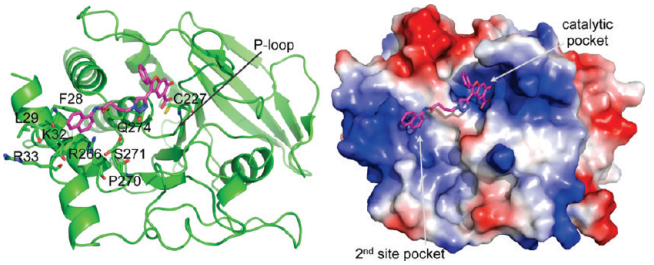


**Figure 1.** Cocrystal structure of Lyp with inhibitor **478** (PDB code 2QCT). Left panel: Ribbon diagram of Lyp catalytic domain with **478** in stick representation (magenta). The catalytic cysteine (C227) as part of the P-loop and amino acid residues that define the second binding site are highlighted in stick representation. Right panel: Same view as left but with Lyp shown in surface representation, colored by electrostatic potential (red, most negative; blue, most positive). The protein structure was corrected by adding the missing side chains for 10 residues as predicted with Schrödinger Prime in the presence of ligand. The structure of the ligand (**478**) was corrected by adding the missing phenyl ring in the 2-position of the benzofuran ring, correcting the valency of the triazole ring, and deprotonating the salicylic acid group. The protein−ligand complex was then minimized with Schrödinger Macromodel (force field, OPLS-2005; solvent, water; dielectric constant = 1; constraints, naphthalene ring and benzofurane ring kept fixed during minimization). The graphics were prepared in PyMol (http://www.pymol.org/).

**Scheme 1.** Click Chemistry Synthesis Scheme of Benzofuran Salicylic Acids

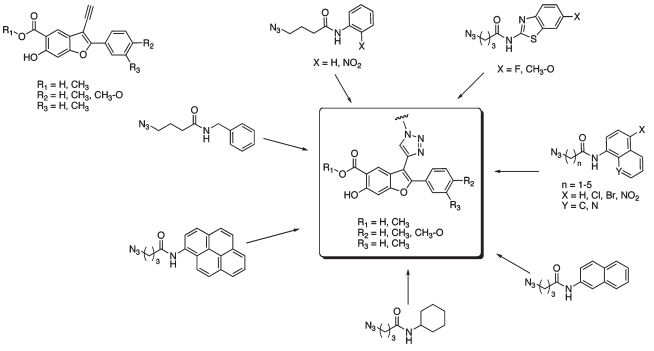


2-position (Scheme 1), which interestingly is not resolved in the cocrystal structure. Since this is probably due to flexibility of the ring, additional substituents in $R_2$- or $R_3$-position could improve affinity for Lyp. To synthesize such a focused library, we employed a click chemistry[14] approach generating a total of 34 compounds (Scheme 1, Table 1). Five different alkynes, containing the benzofuran salicylic acid substructure with different substituents at the phenyl ring, and a variety of azides were chosen for the synthetic scheme (Scheme 1). The alkynes (2-substituted 3-ethynylbenzo[*b*]furans) were synthesized via palladium/copper-catalyzed cross-coupling of *o*-iodoanisoles and ethynylbenzenes, followed by electrophilic cyclization with iodine and another cross-coupling reaction with ethynyltrimethylsilane (Scheme 2). The azides were synthesized as shown in Scheme 3; methyl 4-bromobutanoate (**8**) reacted with sodium azide to yield methyl 4-azidobutanoate (**9**), which was converted into 4-azidobutanoyl chloride (**10**), before coupling with a variety of amines to obtain the corresponding amides (**11**). The final compounds were synthesized via copper-catalyzed click chemistry as shown in Scheme 4.

**Scheme 2.** Chemical Synthesis of the Alkynes

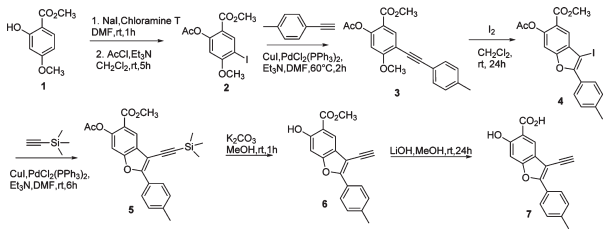


**Scheme 3.** Chemical Synthesis of the Azides

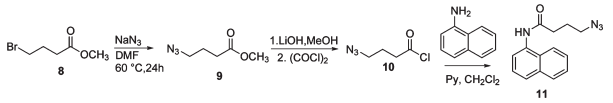


**Scheme 4.** Example of Cu-Catalyzed Click Chemistry Assembly of Final Compounds

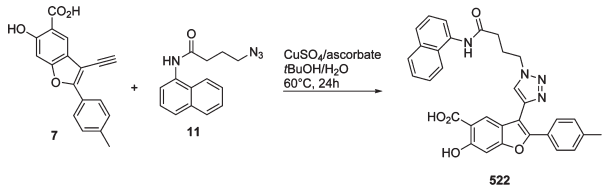


**In Vitro Characterization and Structure−Activity Relationship (SAR) of Benzofuran Salicylic Acids.** A 96-well format phosphatase assay was used to determine $IC_{50}$ values for the synthesized compounds against recombinant Lyp. The assay follows the hydrolyzation of 6,8-difluoro-4-methylumbelliferyl phosphate (DiFMUP), a coumarin-based artificial substrate that turns into a strong fluorophore when dephosphorylated. The $IC_{50}$ value for the original compound **478** (Table 1) was determined to be 4.50 $\mu$M, which is in very good agreement with the reported value of 4.60 $\mu$M.[10] Table 1 lists the $IC_{50}$ values for all synthesized compounds, the majority of which inhibited Lyp to a better extent than **478**. In fact, the top five compounds exhibited $IC_{50}$ values that were more than an order of magnitude lower. Compound **526** ($IC_{50}$ = 0.27 $\mu$M) was the most effective Lyp inhibitor we synthesized, improving inhibitory activity by 17-fold over the original compound **478**. Compared to **478**, **526** carries an additional methyl substituent in the para-position at the phenyl ring ($R_2$), and a bromine substituent at the naphthalene ring. In contrast, **522** ($IC_{50}$ = 0.41 $\mu$M), which contained the additional methyl group but was lacking the bromine atom, was less active, as was **482** ($IC_{50}$ = 0.71 $\mu$M), which carried the bromine substituent but not the methyl group. Thus, most of the gained inhibitory activity of **526** could be attributed to the methyl substituent at the phenyl ring. The methyl group could be replaced by a methoxy substituent without losing notable potency (**584** and **586**, $IC_{50}$ = 0.34 $\mu$M). Similar inhibition as observed for **526** was also found for **525** ($IC_{50}$ = 0.38 $\mu$M), in which a chlorine atom replaced the bromine. In the case of a nitro group substituted naphthalene ring (**524**, $IC_{50}$ = 0.64 $\mu$M), inhibition dropped by about 2-fold, compared to the halogen substituted compounds, indicating that differences in polarity or size of the nitro group prevented tighter binding. Regarding the size of the ring system that binds to the second site in Lyp, compounds with a naphthalene ring were in general better inhibitors than

compounds carrying a phenyl (**609**, **610**, **611**, **612**), pyrene (**619**), or a cyclohexene ring (**528**, **491**). Changing the naphthalene ring to a quinoline (**523**, $IC_{50} = 1.11\ \mu M$) resulted in a less potent compound, whereas other heterocycles, such as methoxybenzothiazole (**630**, $IC_{50} = 0.52\ \mu M$) or fluorobenzothiazole (**636**, $IC_{50} = 0.61\ \mu M$), were better accepted but did not improve inhibitory activity compared to compounds carrying the naphthalene ring. The length of the linker between the triazole moiety and the naphthalene ring also influenced the activity of the inhibitors. Compounds with a linker of three methylene groups inhibited Lyp better than compounds with a shorter or longer linker. For example, **522** (three methylene groups, $IC_{50} = 0.41\ \mu M$) was a more potent inhibitor than **529** (one methylene group, $IC_{50} = 1.18\ \mu M$), **530** (two methylene groups, $IC_{50} = 1.35\ \mu M$), **531** (four methylene groups, $IC_{50} = 2.01\ \mu M$), or **532** (five methylene groups, $IC_{50} = 1.80\ \mu M$). Taking these results together, a single substitution with a methyl or methoxy group at the para-position of the phenyl ring improved the potency of the original inhibitor **478** by an order of magnitude. Additional benefits for binding of the compound to the protein could be achieved by adding a halogen substituent to the naphthalene ring that interacts with the second binding-site in Lyp.

**In Silico Docking of Benzofuran Salicylic Acids.** To study the molecular basis for the improved inhibition of Lyp by our compounds, we used in silico docking and the cocrystal structure of Lyp and **478** (PDB code 2QCT). In particular, we analyzed the effect of the substituents in the para-position at the phenyl ring ($R_2$-position). For the computational analysis, three compounds were chosen that only differed in $R_2$: **584** (methoxy group), **522** (methyl group), and **478** (no substituent). First, the crystal structure was prepared and optimized for the purposes of docking. Both the protein and ligand were corrected and prepared for docking. Side chain conformations of Lys-32 and Lys-42 were predicted followed by minimization, and the molecular structure of **478** was corrected for the missing phenyl ring (see Materials and Methods). On the basis of the assumption that both **478** and its analogues bind similarly to the Lyp active site, we constrained compound binding modes to the corresponding position of **478**. However, unconstrained docking was also performed. Interestingly, the better docking scores were obtained with the constrained docking parameters, suggesting that **584** and **522** indeed bind Lyp similarly to **478**. The docking scores were in very good agreement with the experimental results, ranking **584** at the top with a slightly better score than **522**, while **478** docked with the lowest score among them. To understand the differences in binding affinities, we analyzed the docking poses for specific ligand−protein interactions (Figure 2). These studies revealed that the methoxy group of **584** is in an ideal position to undergo polar−polar interactions with the two side chains of Asp-195 and Glu-277, positioned in the WPD-loop and α6-helix, respectively. It appears feasible that water molecules mediate hydrogen bonding interactions between the oxygen atom of the methoxy group and the carboxylic acid groups of Asp-195 and Glu-277. Such interactions would explain the higher potency of compound **584** compared to **522** and **478** that do not carry polar substituents at the phenyl ring. However, the methyl group of **522**, although nonpolar, can develop an induced dipole due to its polarizability,[15] which could explain favorable interactions with the polar surrounding residues, and may contribute to the higher potency of **522** vs **478**. On the other hand, the methyl group in **522** could also undergo hydrophobic interactions, in particular with the methylene groups of the side chain of Glu-277. Taken together, the in silico docking studies with our inhibitors and Lyp's crystal structure provided a reasonable explanation for the higher activity of compounds with additional substituents in para-position at the phenyl ring ($R_2$).

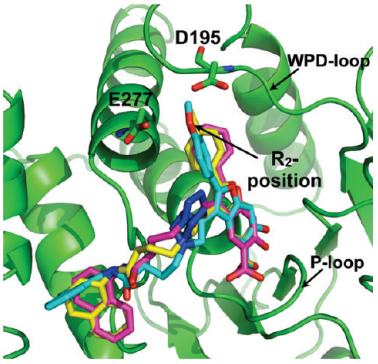


**Figure 2.** In silico docking studies with the crystal structure of Lyp (PDB code 2QCT): docking poses of compounds **584** (cyan), **522** (yellow), and **478** (magenta). Substituents in the para-position ($R_2$) of the phenyl ring in **584** (methoxy) and **522** (methyl) favorably interact with side chains of Asp-195 and Glu-277. Protein structures were prepared with Prime, and docking was performed with Glide (Schrödinger Suite 2009; Schrödinger, LLC). The graphics were prepared in PyMol (http://www.pymol.org/).

**Screening of Compounds in T Cell-Based NFAT/AP-1 Reporter Assays.** Our goal was to generate compounds that could penetrate cell membranes and inhibit Lyp inside living cells. Therefore, we set out to test the synthesized library in T cell-based assays. An ideal screening system to test many compounds is the Jurkat TAg T cell line, on which TCR-induced reporter assays could be easily conducted. The assay employed was based on the expression of a firefly luciferase controlled by the proximal interleukin-2 (IL-2) promoter containing binding sites for nuclear factor of activated T-cells (NFAT) and activator protein 1 (AP-1).[16] A Renilla luciferase under the control of a null-promoter represented the baseline transcriptional activity and was used as a control for unspecific effects on the cellular transcriptional machinery. Because Lyp is a negative regulator of TCR-induced signaling, Lyp inhibitors were expected to increase NFAT/AP-1 activation compared to a vehicle control. Cells were cotransfected with the two plasmids and 16 h later incubated with 5 μM compounds for 45 min, followed by TCR-stimulation or no further stimulation. After 6 h, cells were lysed, dual luciferase assays were conducted, and firefly/Renilla luciferase ratios were calculated for each sample. Since we were interested in compounds that could reverse the inhibitory effects of Lyp on TCR-mediated responses, compounds yielding higher luciferase ratios in the unstimulated vs TCR-stimulated sample were discarded from further evaluation. Compounds giving firefly/Renilla luciferase ratios more than 2-fold higher than the vehicle control (DMSO) were selected for retesting in a dose-response format, using a similar assay setup. The original inhibitor **478** did not show an effect on NFAT/AP-1 activation at the given concentration of 5 μM (Figure 3A). The best inhibitor from the in vitro phosphatase assay (**526**) substantially augmented signaling in the unstimulated sample, while effects in response to TCR stimulation were modest. Interestingly, the same was true for compound **482**; both **526** and **482** contain a bromine substituent at the naphthalene ring. Compounds **486**, **495**, **496**,

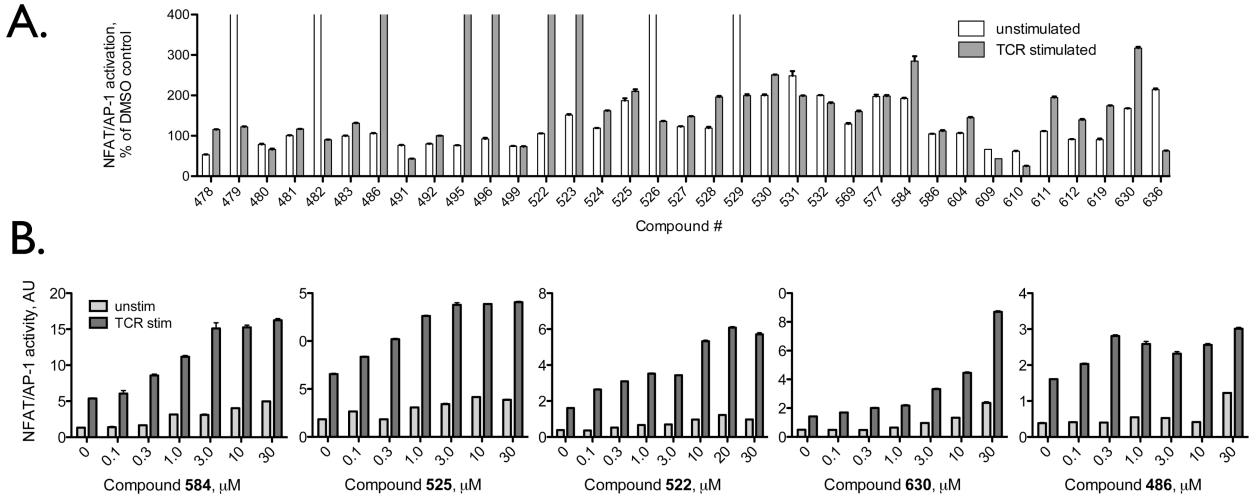


**Figure 3.** Dual luciferase reporter assays in Jurkat TAg T cells to measure the effects of Lyp inhibitors on TCR-induced activation of the proximal IL-2 promoter (containing NFAT and AP-1 sites). (A) Screening of generated benzofuran salicylic acids at 5 $\mu$M. Compounds giving over 2-fold (200%) NFAT/AP-1 activation in the TCR-stimulated sample, compared to a DMSO control, were considered as hits. Compounds yielding higher levels of transcriptional activity in the unstimulated vs TCR-stimulated sample were discarded because of unspecific effects. (B) Dose-response studies of compounds **584**, **525**, **522**, **630**, and **486** on TCR-induced NFAT/AP-1 activation. All samples were run in triplicate (average ± standard deviation), and values are relative to a TCR-stimulated control sample pretreated with DMSO (vehicle control).

**522**, **523**, **525**, **530**, **584**, and **630** showed considerably higher NFAT/AP-1 activation compared to the DMSO control in the TCR-stimulated sample and were chosen for dose-response experiments at concentrations varying from 0.1 to 30 $\mu$M. Compounds **584**, **525**, **522**, **630**, and **486** exhibited a dose-dependent effect (Figure 3B), whereas the remaining compounds (**495**, **496**, **523**, **530**) did not and therefore were discarded from further analysis (data not shown). Notable responses at submicromolar compound concentrations were observed for **584**, **525**, **522**, and **486** (Figure 3B). In the case of compound **630**, NFAT/AP-1 activation was augmented only at $\geq 3\,\mu$M. However, there was a strong increase in activation ($\sim$2.6-fold) between 3 and 30 $\mu$M that was not seen for the other compounds. Interestingly, compound **486**, which was among the least active inhibitors in vitro (Table 1), affected TCR signaling substantially. The chemical structure of **486** is different from all other compounds in that the salicylic acid is esterified with methanol. According to the crystal structure,[10] the free salicylate of **478** mimics the phosphotyrosine (*p*Tyr) of the natural substrate and strongly binds to the phosphate-binding loop (P-loop) at the bottom of the catalytic pocket. In contrast, an uncharged salicylic acid methyl ester cannot bind as strongly to the P-loop, and consequently, in vitro activity of **486** was about 1 order of magnitude lower, compared to the corresponding free acid ($IC_{50} = 4.86\,\mu$M for **486** vs $IC_{50} = 0.56\,\mu$M for **481**). However, better cell-based activity of **486** compared to inhibitors with similar $IC_{50}$ values (e.g., **478**) could be explained with better membrane permeability of the ester vs the free acid. Taken together, out of the 34 compounds tested, 5 inhibitors (**584**, **525**, **522**, **630**, **486**) were found to dose-dependently augment TCR signaling and were chosen for more elaborate assays, in which we probed for Lyp's direct targets immediately downstream of the TCR.

**Effects of Inhibitors on Lyp's Substrates Lck-*p*Y394 and *p*ζ-chain.** Lyp's two most proximal targets relative to the TCR include a tyrosine residue in the activation loop of the Src-kinase Lck (*p*Y394) and the phosphorylated ITAMs of the CD3 and ζ-chains associated with the TCR. Bona fide Lyp inhibitors should affect TCR-induced tyrosine phosphorylation of these signaling molecules. To test this, Jurkat TAg T cells were incubated with compounds **584**, **525**, **522**, **630**, and **486** at 37 °C for 45 min, followed by TCR-stimulation for various time periods. Subsequent immunoblotting revealed that all compounds clearly augmented phosphorylation levels of Lck-*p*Y394 and *p*ζ-chain upon TCR stimulation, compared to the DMSO control (Figure 4). **584** and **486** augmented *p*Tyr levels of Lyp's direct substrates at concentrations as low as 3 and 5 $\mu$M, respectively. Substantial effects of **522** were observed at 10 $\mu$M, whereas 30 $\mu$M compound was needed to observe a genuine effect for **525** and **630**. In particular for **630**, this result corresponded with the data of the NFAT/AP-1 reporter assay (Figure 3B), where **630** was found to be much more active at 30 $\mu$M compared to the lower concentrations tested. Taken together, the downstream effects of the inhibitors on the activation of the IL-2 promoter were found to correlate with augmented phosphorylation levels of Lyp's direct substrates.

In addition to Lck's positive regulatory site (*p*Y394), we also assessed the effects of the compounds on the phosphorylation status of its key negative regulatory residue Tyr-505. This residue is not a direct substrate for Lyp but is rather dephosphorylated by CD45, leading to a conformational change and increased catalytic activity of Lck. As can be seen in Figure 4, Lck-*p*Y505 levels were mainly unaltered in the presence of the inhibitors compared to the DMSO control. However, it should be pointed out that capturing changes in Y505 phosphorylation is generally more difficult because of the high basal phosphorylation levels at this residue. In resting T cells approximately 50% of all Lck molecules are phosphorylated at Y505, and Y505 phosphorylation is at least 15-fold more prevalent than phoshporylation on Y394.[17−20] Nonetheless, given that the inhibitors clearly augment TCR signaling, we can exclude substantial inhibition of CD45-mediated Y505 dephosphorylation by our compounds, which would have led to a decreased TCR response.

**Inhibitor Selectivity Studies.** One of the major hurdles in designing PTP inhibitors as drug candidates remains the relatively low selectivity of compounds for a particular member of this family. Thereby, it is especially difficult to achieve selectivity among structurally similar PTPs,

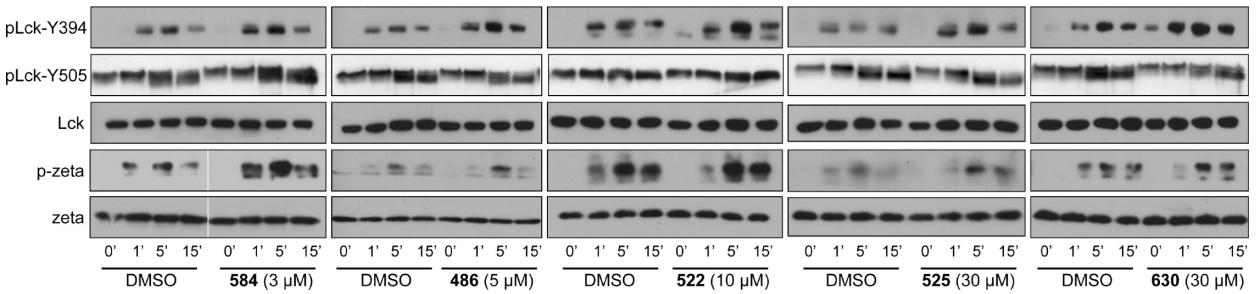


**Figure 4.** Effects of compounds on Lyp's direct substrates Lck-*p*Y394 and the phosphorylated ITAMs of the ζ-chains associated with the TCR, as well as on Lck's negative regulatory site *p*Y505, which is controlled by the CD45 phosphatase. Jurkat TAg T cells were treated with inhibitor or vehicle (DMSO) for 45 min and then TCR-stimulated with OKT3 for 0−1−5−15 min. Subsequently, cell extracts were subjected to immunoblotting with the indicated antibodies.

**Table 2.** Selectivity Studies of Lyp Inhibitors with Closely Related Tyrosine Phosphatases

| | $IC_{50}$, μM | | | | |
|---|---|---|---|---|---|
| | **584** | **525** | **522** | **630** | **486** |
| Lyp | 0.342 | 0.384 | 0.409 | 0.520 | 4.86 |
| PTP1B | 0.190 | 0.205 | 0.214 | 0.217 | 11.5 |
| Shp1 | 0.335 | 0.378 | 0.408 | 0.486 | 5.76 |
| CD45 | 0.410 | 1.05 | 0.681 | 0.877 | 16.2 |
| HePTP | 3.70 | 3.69 | 4.07 | 6.36 | 32.0 |
| LAR | 25.5 | 23.7 | 36.1 | 39.9 | 44.4 |

e.g., among classical *p*Tyr-specific enzymes. Often, this results in unwanted side effects when compounds are tested in rodents or even later in clinical trials as seen for PTP1B inhibitors.[21] To determine selectivity of all the compounds that were active in our cellular assays, we tested them against a panel of closely related PTPs, including PTP1B, Shp1, CD45, HePTP, and LAR (Table 2). Results show that all inhibitors were selective for Lyp over HePTP and LAR by about 1−2 orders of magnitude and over CD45 by up to 3.3-fold. On the other hand, selectivity over PTP1B and Shp1 was in general poor. However, there was one exception to the general trend; **486**, the salicylic acid methyl ester, was indeed selective in inhibiting Lyp over PTP1B by 2.4-fold. Selectivity over Shp1 and CD45 was also better for **486**, compared to the other compounds.

In order to understand the apparent beneficial effect of the methyl ester vs the free salicylic acid, we used in silico docking to compare the binding modes of **486** within the active sites of Lyp and PTP1B (Figure 5). Since the flexible WPD-loop, which contains the catalytic acid/base aspartate, adopts an open conformation in the Lyp cocrystal structure (PDB code 2QCT), we also used an open conformation structure of PTP1B (PDB code 2CM2) for docking. As expected, **486** exhibited a lower docking score in binding to Lyp compared to its free acid analogue. This was due to less favorable electrostatic and van der Waals interactions of the methyl ester with residues of the P-loop and was in agreement with the lower inhibitory activity of **486**, compared to the free acid analogues. More importantly, however, these results suggested that **486** interacts with PTP1B very differently from its binding mode with Lyp. Steric constraints within the PTP1B active site prevent the salicylate ester of **486** from binding to the P-loop of the catalytic pocket. Rather, the ester moiety was found near residues of the open WPD-loop. The naphthalene moiety, which is rotated about its axis, pointed into the opposite direction, compared to its position in Lyp (Figure 5). In general, the docking results suggested that in the case of PTP1B, **486** interacts with residues that are further away from the catalytic center, which may explain the weaker potency of this compound toward PTP1B.

## Discussion and Conclusions

In this study we employed a structure-based approach to generate a focused library of potential Lyp inhibitors, based on the previously reported compound **478** and its cocrystal structure with Lyp.[10] Interestingly, **478** binds Lyp in an open conformation with the WPD-loop in distal position, a PTP inhibitor-binding mode that so far has been recognized only for Lyp and PTP1B.[10,22,26] Our compounds were tailored around the 6-hydroxy-2-phenylbenzofuran-5-carboxylic acid pharmacophore structure of **478**. Specifically, we created compounds with potentially improved affinity toward a second-site binding pocket in Lyp, as well as compounds with additional substituents at a phenyl ring that seemed to have some flexibility in binding to Lyp. Using a click chemistry approach, we synthesized 34 molecules that were first subjected to direct measurements of Lyp inhibition. Thirty compounds inhibited recombinant Lyp to a better extent than **478**. The best compound in the in vitro assay was **526** with an $IC_{50}$ value of 0.27 μM, improving inhibitory activity by 17-fold over the original compound. Compared to **478**, **526** carries additional methyl and bromine substituents at the phenyl and the naphthalene ring, respectively. These rather small additions conferred a greatly improved binding affinity toward both the catalytic pocket and the second-site binding pocket. In particular, the methyl group in para-position ($R_2$) at the phenyl ring contributed most to the improved inhibitory activity of **526**. In silico docking studies with compounds **584**, **522**, and **478** that only differed in the $R_2$ position suggested additional polar−polar and/or van der Waals interactions of the methyl (**522**) or methoxy (**584**) group with the side chains of amino acid residues Asp-195 and Glu-277. In contrast, **478**, which does not contain a substituent in $R_2$, cannot make such additional favorable interactions with these residues that are part of the WPD-loop and the α6-helix, respectively, at the edge of Lyp's catalytic pocket in open conformation.

Importantly, we found several lines of evidence that our compounds could penetrate cell membranes and inhibit Lyp's enzymatic activity in live T cells. First, NFAT/AP-1 reporter assays revealed that nine of the 34 compounds augmented downstream TCR signaling at least 2-fold. Pivotal for a genuine effect on Lyp activity, five of these nine compounds (**584**, **525**, **522**, **630**, **486**) acted in a dose-dependent manner. Notably, compounds with a bromine substituent at the naphthalene ring (**526**, **482**) enhanced T cell signaling in a non-TCR-mediated manner and were therefore omitted from further consideration.

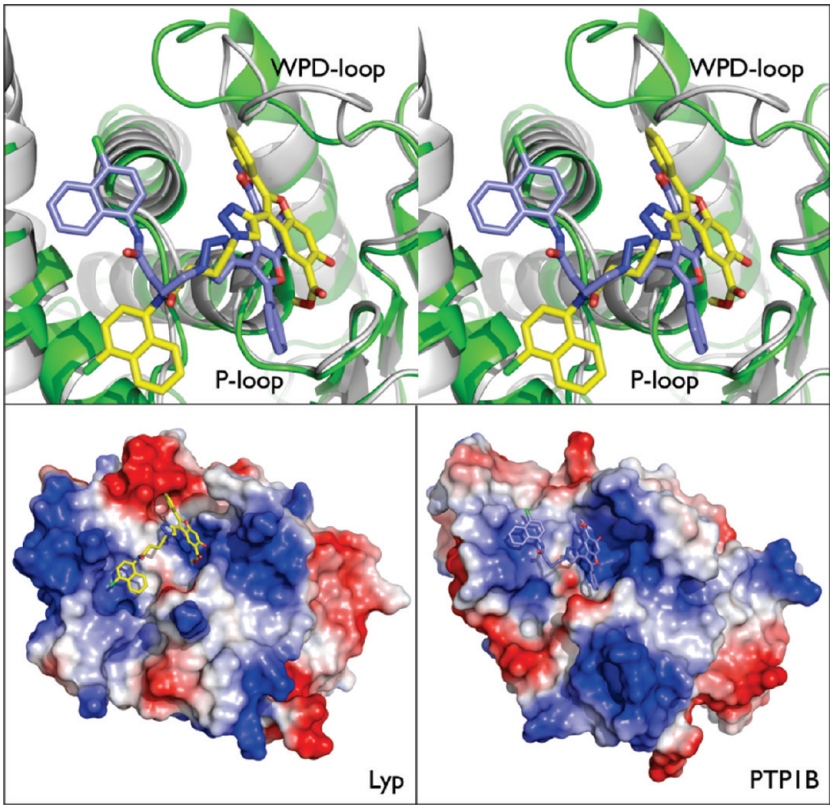


**Figure 5.** In silico docking studies with compound **486** and the crystal structures of Lyp (PDB code 2QCT) and PTP1B (PDB code 2CM2). Upper panel: Stereoribbon diagram close-up of active sites of Lyp (green) and PTP1B (white) with docking poses for **486** in stick representation (with Lyp, yellow; with PTP1B, blue). Lower panel: Lyp and PTP1B shown in surface representation, colored by electrostatic potential (red, most negative; blue, most positive). Docking poses for **486** in stick representation as above. Protein structures were prepared with Prime, and docking was performed with Glide (Schrödinger Suite 2009; Schrödinger, LLC). The graphics were prepared in PyMol (http://www.pymol.org/).

Also, compounds with a nitro group at this position did not show cell activity, maybe because of lack of membrane permeability. Second, TCR-induced phosphorylation of Lyp's direct targets Lck-*p*Y394 and *pζ*-chain was enhanced in cells pretreated with the mentioned five compounds, confirming that their effects on TCR signaling is due to inhibition of Lyp activity. Interestingly, compound **486**, the only ester we synthesized, showed very good activity in the cell assays, although inhibition of recombinant Lyp was relatively modest. This was probably due to improved membrane permeability of the ester compared to compounds with a free salicylic acid and consequently a higher effective concentration of **486** inside the cell compared to its negatively charged analogues. Alternatively, the ester in **486** might also get quickly hydrolyzed inside the cell, generating a more active compound. Further studies will be necessary to determine the exact mechanism in cells.

Profiling studies against a panel of five closely related phosphatases showed that our inhibitors indeed are selective for Lyp over CD45 and, especially, over HePTP and LAR. Poor selectivity of most compounds over Shp1 and PTP1B underlines once more the challenge in generating monoselective PTP inhibitors. In particular for PTP1B, which also comprises a second-site binding pocket and similar residues in the WPD-loop and α6-helix, in silico docking experiments suggested that most compounds adopt a binding mode that is similar to Lyp (data not shown). More interestingly, however, we found that compound **486** exhibited a much better selectivity for Lyp over the other phosphatases, including PTP1B and Shp1. According to the in silico docking, the ester group in **486** is able to bind to the P-loop region in Lyp while steric constraints within the active site does not allow a similar binding mode in PTP1B. In Lyp's open conformation, the WPD-loop adopts an unusually distant position,[23] resulting in a larger binding site compared to other PTPs, including PTP1B. With this additional space, Lyp can better accommodate the sterically more demanding ester compound, whereas in a similar position in PTP1B, the phenyl ring of **486** would collide with residues of the WPD-loop. Whether the in vitro selectivity of **486** is relevant in cells or in vivo will depend on the stability of the ester under physiological conditions. Thus, further studies are warranted to determine the pharmacokinetic properties of this compound and maybe additional esters of the most potent free acid analogues.

In conclusion, we have successfully applied a structure-based approach to design a library of Lyp inhibitors with substantially improved potency, compared to a known compound. Several of these molecules were able to inhibit Lyp in live T cells at low micromolar concentrations. We also provide evidence of how selectivity for Lyp as well as cell-based activity could be improved in future compounds, which may become useful for the treatment of autoimmunity.

## Materials and Methods

**Reagents, Antibodies, Plasmids, and Recombinant PTPs.** 6,8-Difluoro-4-methylumbelliferyl phosphate (DiFMUP) was from Invitrogen Inc. (Carlsbad, CA). PEG8000 was from Sigma-Aldrich (St. Louis, MO). All other chemicals and reagents were

of the highest grade available commercially. Anti-Lck and anti-ζ chain antibodies were purchased from Santa Cruz Biotechnology. Anti-HA was purchased from Covance Inc., anti-Lck phosphotyrosine-394 from Cell Signaling Technology, and anti-LAT from Upstate/Millipore. Monoclonal antibodies against phosphotyrosine (4G10) and CD3ε (OKT3) were purified from hybridomas grown in our laboratory. All plasmids have been reported before.[9,24,25] Recombinant Lyp catalytic domain (residues 2−309) and HePTP were expressed and purified as previously described.[26,27] Recombinant PTP1B, Shp1, CD45, and LAR were purchased from BIOMOL Research Laboratories, Inc. (Plymouth Meeting, PA).

**Chemical Syntheses: General.** All reactions sensitive to air or moisture were carried out under argon atmosphere in oven-dried glassware unless otherwise noted. All reagents were purchased from Sigma-Aldrich and were used as supplied unless otherwise stated. For column chromatography, silica gel 60 (230−400 mesh) was used. $^1$H and $^{13}$C NMR spectra were recorded on a Varian 300 MHz spectrometer. Chemical shifts are reported in ppm from tetramethylsilane with reference to internal residual solvent. The following abbreviations are used to designate the signal multiplicities: s = singlet, d = doublet, dd = doublet of doublet, t = triplet, and m = multiplet. Coupling constants are reported in hertz (Hz). High-resolution mass spectrometry (HRMS-FAB) spectra were obtained using a JMS-HX110A mass spectrometer (JEOL, Tokyo, Japan). The purity of the compounds was >95%.

**Methyl 2-Acetoxy-5-iodo-4-methoxybenzoate (2).** To a solution of 1.82 g (10 mmol) of methyl 2-hydroxy-4-methoxybenzoate (**1**) and 1.80 g (12 mmol) of NaI in 20 mL of DMF at 25 °C was added 3.38 g (12 mmol) of chloramine T trihydrate. The mixture was stirred for 1 h. The product was diluted with water, acidified with 5% hydrochloric acid solution, and extracted with ethyl acetate. The organic solution was washed successively with 5% sodium thiosulfate solution and brine and was dried over anhydrous sodium sulfate. The solvent was removed under reduced pressure, and the residue was dissolved in 50 mL of methylene chloride and 5 mL (35 mmol) of triethylamine. Then 1.76 g of acetyl chloride in 5 mL of methylene chloride was added dropwise. The mixture was stirred for 5 h at room temperature. The reaction was quenched by adding 10 mL of water and extracted with methylene chloride. The organic solution was washed with brine, dried over anhydrous sodium sulfate. The solvent was removed to get 3.06 g of **2** as a white solid, which was used without further purification.

**Methyl 2-Acetoxy-4-methoxy-5-(phenylethynyl)benzoate (3).** To a solution of 2 g (5.7 mmol) of **2** and 0.87 g (8.5 mmol) of ethynylbenzene in 10 mL of DMF was added 22 mg (0.11 mmol) of CuI, 160 mg (0.23 mmol) of $PdCl_2(PPH_3)_2$, and 2 mL (14 mmol) of $Et_3N$. The mixture was stirred at 60 °C for 2 h. Then 20 mL of 1 N HCl was added, and a precipitate was formed. The product was extracted by ether. The ether phase and solid were combined, and the solvent was removed under reduced pressure. Recrystallization from methanol yielded 1.41 g of **3** as brown solid.

**Methyl 6-Acetoxy-3-iodo-2-phenylbenzofuran-5-carboxylate (4).** To a solution of 1.30 g (4 mmol) of **3** in 50 mL of methylene chloride was added 3.8 g (15 mmol) of iodine in 50 mL of methylene chloride at 0 °C. The mixture was stirred at 0 °C for 30 min and allowed to warm to room temperature and stirred overnight. Then 30 mL of concentrated $Na_2S_2O_3$ solution was added to remove the excess iodine, and the appropriate layer was extracted with methylene chloride. The organic phase was dried, and the solvent was removed. Purification by chromatography gave 0.87 g of **4** as red-brown solid.

**Methyl 6-Acetoxy-2-phenyl-3-((trimethylsilyl)ethynyl)benzofuran-5-carboxylate (5).** Compound **5** was synthesized similarly to compound **3**. The product was purified by chromatography.

**3-Ethynyl-6-hydroxy-2-phenylbenzofuran-5-carboxylic Acid (7).** To a solution of 122 mg (0.3 mmol) of **5** in 5 mL of methanol was added 90 mg (0.6 mmol) of $K_2CO_3$. The mixture was stirred for 1 h at room temperature, and the solvent was removed. Purification by chromatography gave compound **6**, which was dissolved in 5 mL of methanol. Water was added dropwise until the solution became cloudy. Then 200 mg of LiOH was added and the mixture was stirred overnight. After removal methanol, 10 mL of 1 N HCl was added and extracted with ethyl acetate. The organic phase was dried and the solvent was removed to obtain 51 mg of **7** as a brown solid.

**Methyl 4-Azidobutanoate (9).** To a solution of 1.81 g (10 mmol) of **8** in 5 mL of DMF was added 2.60 g (40 mmol) of $NaN_3$. The mixture was stirred at 60 °C for 24 h. The product was diluted with water and extracted with ether. The organic phase was washed with brine and dried over sodium sulfate. The solvent was removed to obtain 1.23 g of **9** as light yellow liquid.

**4-Azido-*N*-(naphthalen-1-yl)butanamide (11).** To a solution of 1 g (7.0 mmol) of **9** in 10 mL of methanol was added water until the solution became cloudy. Then 500 mg of LiOH was added and the mixture was stirred at room temperature for 24 h. The methanol was removed, and 10 mL of 3 N HCl was added. The appropriate layer was extracted with ethyl acetate. The solvent was removed to get the free acid, which was stirred with 2 mL of $(COCl)_2$ and 20 mL of methylene chloride. Then 1 drop of DMF was added to catalyze the reaction. The mixture was stirred for 3 h. The solvent was removed to get the acid chloride **10**. And compound **10** was dissolved in 5 mL of methylene chloride, which was added dropwise to a solution of 1 g (7.0 mmol) of naphthalen-1-amine and 2 mL (14 mmol) of triethyamine in 10 mL of ethylene chloride. The mixture was stirred at room temperature for 3 h and washed with water to get 1.51 g of crude **11** as an off-white solid.

**6-Hydroxy-3-(1-(4-(naphthalen-1-ylamino)-4-oxobutyl)-1*H*-1,2,3-triazol-4-yl)-2-*p*-tolylbenzofuran-5-carboxylic Acid (522).** To a solution of 20 mg of **7** and 20 mg of **11** in 1 mL of water and 1 mL of *t*-BuOH was added 34 mg of $CuSO_4 \cdot 5H_2O$ and 27 mg of sodium ascorbate. The mixture was stirred at 60 °C for 24 h. The solvent was removed and the residue was purified by chromatography to give 27 mg of **522** as an off-white solid. $^1$H NMR ($CDCl_3$/$CD_3OD$) δ 8.14 (s, 1H), 7.74 (m, 2H), 7.63 (m, 1H), 7.52 (m, 1H), 7.46 (d, 1H, $J$ = 8.1 Hz), 7.28 (m, 4H), 7.01 (d, 1H, $J$ = 8.1 Hz), 6.86 (s, 1H), 4.43 (m, 2H), 2.46 (m, 2H), 2.22 (m, 2H), 2.16 (s, 3H); $^{13}$C NMR ($CDCl_3$/$CD_3OD$) δ 172.5, 172.3, 169.4, 157.9, 152.6, 139.4, 134.3, 132.6, 129.4, 128.5, 128.4, 127.3, 127.1, 126.6, 126.3, 126.1, 125.5, 123.2, 122.7, 122.1, 121.7, 106.3, 98.4, 50.0, 33.0, 26.4, 21.4. HRMS (FAB) cacld for $C_{32}H_{27}N_4O_5$ $(M + H)^+$ $m/z$ 547.1981, found 547.1980.

**Methyl 3-(1-(4-(4-Chloronaphthalen-1-ylamino)-4-oxobutyl)-1*H*-1,2,3-triazol-4-yl)-6-hydroxy-2-phenylbenzofuran-5-carboxylate (486). 486** was synthesized similarly to **522**. $^1$H NMR ($CDCl_3$/$CD_3OD$) δ 8.28 (s, 1H), 8.20 (d, 1H, $J$ = 7.5 Hz), 7.95 (d, 1H, $J$ = 7.5 Hz), 7.91 (s, 1H), 7.70 (m, 2H), 7.55 (m, 3H), 7.37 (m, 4H), 7.06 (s, 1H), 4.61 (t, 2H, $J$ = 6.6 Hz), 3.90 (s, 3H), 2.63 (t, 2H, $J$ = 6.9 Hz), 2.40 (m, 2H); $^{13}$C NMR ($CDCl_3$/$CD_3OD$) δ 184.9, 172.5, 169.4, 160.1, 132.0, 129.7, 129.5, 128.8, 127.3, 127.0, 125.8, 124.9, 123.3, 122.6, 99.0, 91.5, 52.4, 34.4, 32.9, 23.0. HRMS (FAB) cacld for $C_{32}H_{26}ClN_4O_5$ $(M + H)^+$ $m/z$ 581.1592, found 581.1511.

**3-(1-(4-(4-Chloronaphthalen-1-ylamino)-4-oxobutyl)-1*H*-1,2,3-triazol-4-yl)-6-hydroxy-2-*p*-tolylbenzofuran-5-carboxylic Acid (525). 525** was synthesized similarly to **522**. $^1$H NMR ($CDCl_3$/$CD_3OD$) δ 8.20 (d, 1H, $J$ = 8.7 Hz), 8.16 (s, 1H), 8.02 (s, 1H) 7.95 (d, 1H, $J$ = 8.7 Hz), 7.65 (d, 2H, $J$ = 8.1 Hz), 7.57−7.47 (m, 4H), 7.14 (d, 2H, $J$ = 8.1 Hz), 6.94 (s, 1H), 4.61 (m, 2H), 2.61 (m, 2H), 2.42 (m, 2H), 2.31 (s, 3H); $^{13}$C NMR ($CDCl_3$/$CD_3OD$) δ 172.5, 166.2, 159.6, 156.3, 140.1, 138.9, 131.4, 129.2, 127.2, 127.0, 126.9, 125.7, 124.9, 124.8, 123.5, 122.7, 122.6, 122.4, 97.8, 94.6, 50.0, 32.9, 26.2, 21.3. HRMS (FAB) cacld for $C_{32}H_{26}ClN_4O_5$ $(M + H)^+$ $m/z$ 581.1592, found 581.1549.

**6-Hydroxy-2-(4-methoxyphenyl)-3-(1-(4-(naphthalen-1-ylamino)-4-oxobutyl)-1*H*-1,2,3-triazol-4-yl)benzofuran-5-carboxylic Acid (584). 584** was synthesized similarly to **522**. $^1$H NMR ($CDCl_3$/$CD_3OD$) δ 8.21 (s, 1H), 7.90 (m, 2H), 7.78 (m, 1H), 7.66 (d, 2H, $J$ = 8.7 Hz), 7.60 (m, 1H), 7.40 (m, 4H), 6.96 (s, 1H), 6.86 (d, 2H, $J$

=8.7 Hz), 4.58 (t, 2H, $J$=6.6 Hz), 3.77 (s, 3H), 2.60 (t, 2H, $J$=6.9 Hz), 2.39 (m, 2H); $^{13}$C NMR ($CDCl_3$/$CD_3OD$) $\delta$ 172.1, 160.3, 160.1, 157.6, 152.3, 140.2, 134.3, 132.6, 128.7, 128.4, 126.5, 126.3, 126.1, 125.5, 123.1, 122.9, 122.8, 122.6, 122.0, 121.5, 118.1, 114.2, 105.5, 98.2, 55.5, 33.0, 26.4, 19.1. HRMS (FAB) calcd for $C_{32}H_{27}N_4O_6$ $(M + H)^+$ $m/z$ 563.1931, found 563.1955.

**6-Hydroxy-3-(1-(4-(6-methoxybenzo[*d*]thiazol-2-ylamino)-4-oxobutyl)-1*H*-1,2,3-triazol-4-yl)-2-*m*-tolylbenzofuran-5-carboxylic Acid (630). 630** was synthesized similarly to **522**. $^1$H NMR ($CDCl_3$/$CD_3OD$) $\delta$ 8.25 (s, 1H), 7.80 (s, 1H), 7.53 (m, 2H), 7.46 (d, 1H, $J$ = 7.8 Hz), 7.18 (m, 2H), 7.11 (d, 1H, $J$=7.8 Hz), 6.94 (s, 1H), 6.91 (m, 1H), 4.52 (m, 2H), 3.80 (s, 3H), 2.54 (m, 2H), 2.35 (m, 2H), 2.31(s, 3H); $^{13}$C NMR ($CDCl_3$/$CD_3OD$) $\delta$ 172.5, 170.9, 169.4, 156.8, 142.3, 138.5, 133.1, 130.2, 129.9, 128.6, 127.8, 124.4, 123.0, 121.3, 115.4, 106.7, 104.3, 98.1, 88.4, 60.9, 56.0, 32.3, 25.5, 21.6. HRMS (FAB) cacld for $C_{30}H_{26}N_5O_6S$ $(M + H)^+$ $m/z$ 584.1604, found 584.1619.

**$IC_{50}$ Measurements.** The PTP-catalyzed hydrolysis of DiFMUP in the presence of compound was assayed at 30 °C in a 60 $\mu$L 96-well format reaction system in 50 mM Bis-Tris, pH 6.0 assay buffer having an ionic strength of 50 mM (adjusted with NaCl) and containing 1 mM dithiotreitol, 5% DMSO, and 1% PEG8000. At various concentrations of the compound, the initial rate at fixed DiFMUP concentration (equal to the corresponding $K_m$ value for each PTP) was determined using a FLx800 microplate reader (Bio-Tek Instruments, Inc.), an excitation wavelength of 360 nm and measuring the emission of the fluorescent reaction product 6,8-difluoro-7-hydroxy-4-methylcoumarin at 460 nm. The nonenzymatic hydrolysis of the substrate was corrected by measuring the control without addition of enzyme. The $IC_{50}$ values were calculated as described before.[27]

**In Silico Docking Experiments.** We used the Schrödinger software package for the structure preparations and docking (Schrödinger Suite 2009; Schrödinger, LLC). The crystal structure of Lyp complexed with **478** (PDB accession code 2QCT) was used for the docking studies. Protein and ligand were separated, and their structures were corrected. The missing atoms of the Lyp side chains of Lys-32 and Lys-42 were predicted by Prime, and the resulting (corrected) protein structure was processed using the protein preparation facility in Maestro. The docking grid was generated using Glide, and a hydrogen bond constraint (Gln-274) was included in the grid definition. The **478** structure was corrected for the missing phenyl ring and prepared for redocking by LigPrep in the same way as all ligands. The processed ligand was redocked into the Lyp structure and the new complex minimized using Macromodel with the OPLS-AA force field. Such a minimized Lyp structure was used for ligand docking. Docking calculations were performed in the standard-precision mode with and without constraint and the results evaluated by docking scores and docking poses. In silico docking was also performed using PTP1B for a selected subset of ligands. PDB structures of PTP1B in the open conformation were analyzed, and the structure with the best resolution of 1.50 Å was selected (PDB code 2CM2). Energetically optimized 3D structures for the **478** analogues were generated as starting points for flexible docking using LigPrep. LigPrep enumerates feasible tautomers, protonation states (pH 6 ± 2), generates 3D conformations, and executes a minimization protocol using the OPLS-AA force field.

**Dual Luciferase Assay.** Jurkat TAg T cells were co-transfected by electroporation[9] with a plasmid encoding firefly luciferase (under the control of the proximal IL-2 promoter containing the NFAT and AP-1 sites) and a plasmid encoding Renilla luciferase (under the control of a null-promoter). Sixteen hours later cells were incubated with candidate compounds (at 5 $\mu$M unless otherwise stated) or DMSO alone (vehicle control) for 45 min at 37 °C. Then cells were TCR-stimulated with an optimal dose of OKT3 (500 ng/mL) for 6 h, and reactions were stopped by lysing cells in lysis buffer (from Promega), before being subjected to a dual luciferase assay (Promega) using a luminometer (Veritas Microplate Luminometer, Promega). The level of NFAT/AP-1 activation for a sample was calculated as the ratio between firefly and Renilla luciferase activity for the same sample. Typically, each sample was run in triplicate. Compounds giving firefly/Renilla luciferase ratios >2-fold higher than the corresponding ratios for the control samples (DMSO) were selected for retesting in a dose-response format, using the same assay.

**TCR Time Courses, Cell Lysis, and Immunoblotting.** Jurkat TAg T cells were treated with small-molecule compound or DMSO as described above. Thereafter, cells were TCR stimulated (OKT3, 500 ng/mL) for the indicated time periods and then lysed in lysis buffer (50 mM HEPES, pH 7.4, 100 mM NaCl, 1% Triton X-100, 50 mM NaF, 5 mM $Na_3VO_4$, 1 mM PMSF, 5 mM EDTA). Proteins were later resolved by SDS−PAGE, transferred onto PVDF membranes, and blotted with the indicated antibodies. These procedures were as before.[9]

**Acknowledgment.** This work was supported by Grants 1R21CA132121 (to L.T.) and MLSCN U54 HG003914 (to T.M.) from the National Institutes of Health. Support came also from the Norwegian Cancer Society (to T.V.) and from the Oxnard Foundation. We acknowledge resources of the University of Miami Center for Computational Science (CCS). We also thank Gladys M. Tjørhom and Jorun Solheim for technical assistance and Kjetil Tasken for support.

## References

(1) Alonso, A.; Sasin, J.; Bottini, N.; Friedberg, I.; Friedberg, I.; Osterman, A.; Godzik, A.; Hunter, T.; Dixon, J.; Mustelin, T. Protein tyrosine phosphatases in the human genome. *Cell* **2004**, *117*, 699–711.

(2) Tonks, N. K. Protein tyrosine phosphatases: from genes, to function, to disease. *Nat. Rev. Mol. Cell Biol.* **2006**, *7*, 833–846.

(3) Bialy, L.; Waldmann, H. Inhibitors of protein tyrosine phosphatases: next-generation drugs? *Angew. Chem., Int. Ed.* **2005**, *44*, 3814–3839.

(4) Tautz, L.; Pellecchia, M.; Mustelin, T. Targeting the PTPome in human disease. *Expert Opin. Ther. Targets* **2006**, *10*, 157–177.

(5) Vang, T.; Miletic, A. V.; Arimura, Y.; Tautz, L.; Rickert, R. C.; Mustelin, T. Protein tyrosine phosphatases in autoimmunity. *Annu. Rev. Immunol.* **2008**, *26*, 29–55.

(6) Cohen, S.; Dadi, H.; Shaoul, E.; Sharfe, N.; Roifman, C. M. Cloning and characterization of a lymphoid-specific, inducible human protein tyrosine phosphatase, Lyp. *Blood* **1999**, *93*, 2013–2024.

(7) Wu, J.; Katrekar, A.; Honigberg, L. A.; Smith, A. M.; Conn, M. T.; Tang, J.; Jeffery, D.; Mortara, K.; Sampang, J.; Williams, S. R.; Buggy, J.; Clark, J. M. Identification of substrates of human protein-tyrosine phosphatase PTPN22. *J. Biol. Chem.* **2006**, *281*, 11002–11010.

(8) Bottini, N.; Musumeci, L.; Alonso, A.; Rahmouni, S.; Nika, K.; Rostamkhani, M.; MacMurray, J.; Meloni, G. F.; Lucarelli, P.; Pellecchia, M.; Eisenbarth, G. S.; Comings, D.; Mustelin, T. A functional variant of lymphoid tyrosine phosphatase is associated with type I diabetes. *Nat. Genet.* **2004**, *36*, 337–338.

(9) Vang, T.; Congia, M.; Macis, M. D.; Musumeci, L.; Orru, V.; Zavattari, P.; Nika, K.; Tautz, L.; Tasken, K.; Cucca, F.; Mustelin, T.; Bottini, N. Autoimmune-associated lymphoid tyrosine phosphatase is a gain-of-function variant. *Nat. Genet.* **2005**, *37*, 1317–1319.

(10) Yu, X.; Sun, J. P.; He, Y.; Guo, X.; Liu, S.; Zhou, B.; Hudmon, A.; Zhang, Z. Y. Structure, inhibitor, and regulatory mechanism of Lyp, a lymphoid-specific tyrosine phosphatase implicated in autoimmune diseases. *Proc. Natl. Acad. Sci. U.S.A.* **2007**, *104*, 19767–19772.

(11) Puius, Y. A.; Zhao, Y.; Sullivan, M.; Lawrence, D. S.; Almo, S. C.; Zhang, Z. Y. Identification of a second aryl phosphate-binding site in protein-tyrosine phosphatase 1B: a paradigm for inhibitor design. *Proc. Natl. Acad. Sci. U.S.A.* **1997**, *94*, 13420–13425.

(12) Salmeen, A.; Andersen, J. N.; Myers, M. P.; Tonks, N. K.; Barford, D. Molecular basis for the dephosphorylation of the activation segment of the insulin receptor by protein tyrosine phosphatase 1B. *Mol. Cell* **2000**, *6*, 1401–1412.

(13) Zhang, S.; Zhang, Z. Y. PTP1B as a drug target: recent developments in PTP1B inhibitor discovery. *Drug Discovery Today* **2007**, *12*, 373–381.

(14) Kolb, H. C.; Finn, M. G.; Sharpless, K. B. Click chemistry: diverse chemical function from a few good reactions. *Angew. Chem., Int. Ed.* **2001**, *40*, 2004–2021.
(15) Rice, O. K. *Electronic Structure and Chemical Bonding*; McGraw-Hill: New York, 1940.
(16) Sherf, B. A.; Navarro, S. L.; Hannah, R. R.; Wood, K. V. Dual-luciferase reporter assay: an advanced co-reporter technology integrating firefly and Renilla luciferase assays. *Promega Notes* **1996**, *57*, 02.
(17) Rodgers, W.; Rose, J. K. Exclusion of CD45 inhibits activity of p56lck associated with glycolipid-enriched membrane domains. *J. Cell Biol.* **1996**, *135*, 1515–1523.
(18) Ostergaard, H. L.; Shackelford, D. A.; Hurley, T. R.; Johnson, P.; Hyman, R.; Sefton, B. M.; Trowbridge, I. S. Expression of CD45 alters phosphorylation of the lck-encoded tyrosine protein kinase in murine lymphoma T-cell lines. *Proc. Natl. Acad. Sci. U.S.A.* **1989**, *86*, 8959–8963.
(19) Veillette, A.; Horak, I. D.; Horak, E. M.; Bookman, M. A.; Bolen, J. B. Alterations of the lymphocyte-specific protein tyrosine kinase (p56lck) during T-cell activation. *Mol. Cell. Biol.* **1988**, *8*, 4353–4361.
(20) Hardwick, J. S.; Sefton, B. M. The activated form of the Lck tyrosine protein kinase in cells exposed to hydrogen peroxide is phosphorylated at both Tyr-394 and Tyr-505. *J. Biol. Chem.* **1997**, *272*, 25429–25432.
(21) Erbe, D. V.; Wang, S.; Zhang, Y. L.; Harding, K.; Kung, L.; Tam, M.; Stolz, L.; Xing, Y.; Furey, S.; Qadri, A.; Klaman, L. D.; Tobin, J. F. Ertiprotafib improves glycemic control and lowers lipids via multiple mechanisms. *Mol. Pharmacol.* **2005**, *67*, 69–77.
(22) Liu, S.; Zeng, L. F.; Wu, L.; Yu, X.; Xue, T.; Gunawan, A. M.; Long, Y. Q.; Zhang, Z. Y. Targeting inactive enzyme conformation: aryl diketoacid derivatives as a new class of PTP1B inhibitors. *J. Am. Chem. Soc.* **2008**, *130*, 17075–17084.
(23) Barr, A. J.; Ugochukwu, E.; Lee, W. H.; King, O. N.; Filippakopoulos, P.; Alfano, I.; Savitsky, P.; Burgess-Brown, N. A.; Muller, S.; Knapp, S. Large-scale structural analysis of the classical human protein tyrosine phosphatome. *Cell* **2009**, *136*, 352–363.
(24) Arimura, Y.; Vang, T.; Tautz, L.; Williams, S.; Mustelin, T. TCR-induced downregulation of protein tyrosine phosphatase PEST augments secondary T cell responses. *Mol. Immunol.* **2008**, *45*, 3074–3084.
(25) Methi, T.; Ngai, J.; Mahic, M.; Amarzguioui, M.; Vang, T.; Tasken, K. Short-interfering RNA-mediated Lck knockdown results in augmented downstream T cell responses. *J. Immunol.* **2005**, *175*, 7398–7406.
(26) Wu, S.; Bottini, M.; Rickert, R. C.; Mustelin, T.; Tautz, L. In silico screening for PTPN22 inhibitors: active hits from an inactive phosphatase conformation. *ChemMedChem* **2009**, *4*, 440–444.
(27) Tautz, L.; Bruckner, S.; Sareth, S.; Alonso, A.; Bogetz, J.; Bottini, N.; Pellecchia, M.; Mustelin, T. Inhibition of Yersinia tyrosine phosphatase by furanyl salicylate compounds. *J. Biol. Chem.* **2005**, *280*, 9400–9408.